Quantum transport in non-Hermitian impurity arrays

K. L. Zhang, X. M. Yang, and Z. Song*
School of Physics, Nankai University, Tianjin 300071, China

(Received 14 May 2019; published 15 July 2019)

We study the formation of band gap bound states induced by a non-Hermitian impurity embedded in a Hermitian system. We show that a pair of bound states emerges inside the band gap when a parity-time ($\mathcal{PT}$) imaginary potential is added in strongly coupled bilayer lattices and the bound states become strongly localized when the system approaches the exceptional point. As a direct consequence of such $\mathcal{PT}$ impurity-induced bound states, an impurity array can be constructed and protected by energy gap. The effective Hamiltonian of the impurity array is non-Hermitian Su-Schrieffer-Heeger type and hosts Dirac probability-preserving dynamics. We demonstrate the conclusion by numerical simulations for the quantum transport of wave packet in right-angle bends waveguide and Y-beam splitter. Our finding provides an alternative way to fabricate quantum device by non-Hermitian impurity.

DOI: 10.1103/PhysRevB.100.024305

I. INTRODUCTION

Throughout physics, stable or equilibrium phenomena can be understood by bound state, ranging from quantum to classical objects. In quantum physics, a bound state is a localized state of a particle subject to a real valued potential, which may be the result of the presence of other particles. The concept of bound state is ubiquitous in numerous branches of physics, such as optics and condensed matter. In experiment, engineering bound state can be generated by artificial defects in photonic crystals and an array of defects, which are known as coupled-resonator optical waveguides providing almost lossless guiding, and bending of wave packet [1–11]. By introducing artificial defects, various photonic crystal devices can be realized for the applications in a wide variety of fields. Nowadays a complex potential is not forbidden since non-Hermitian quantum mechanics has emerged as a versatile platform for fabricating functional devices in a non-Hermitian regime. The main mechanism is based on the existence of imaginary potential, which has been investigated theoretically [12–30] and realized in experiment [31–40] as an ideal building block of non-Hermitian systems. A non-Hermitian term has a distinguishing feature that differs from a Hermitian one and can be exemplified by a simple two level system. An extra pseudo-Hermitian non-Hermitian term always shrinks the level spacing, while a nontrivial Hermitian perturbation always leads to the repulsion of the two levels. Presumably, midgap levels can be generated by adding non-Hermitian impurity on a Hermitian gapped system.

In this paper, we study the possibility of a quantum channel generated by an array of non-Hermitian defects. Based on the Bethe ansatz solution we show that a pair of bound states emerges inside the band gap when a parity-time ($\mathcal{PT}$) imaginary potential is added in a strongly coupled bilayer. Such bound states are protected by energy gap, especially as the bound-state energy tends to zero when the system approaches the exceptional point (EP). Consequently, an impurity array can be constructed in the midgap and provides a low-loss waveguide since other Hermitian degrees of freedom are adiabatically eliminated when we consider the dynamics in the impurity array. In addition, we show that the effective Hamiltonian of the impurity array is equivalent to a non-Hermitian Su-Schrieffer-Heeger (SSH) system and obeys chiral-time ($\mathcal{CT}$) symmetry. This ensures quasiorthogonality of the midgap modes in the framework of Dirac inner product, and therefore the Dirac probability-preserving dynamics in the waveguide. Therefore, although the waveguide is engineered by non-Hermitian impurities, it acts as a conditional Hermitian device. We demonstrate the conclusion by numerical simulations for the quantum transport of wave packet in right-angle bends waveguide and Y-beam splitter. Our finding provides an alternative way to fabricate quantum device by non-Hermitian impurity.

This paper is organized as follows. In Sec. II, we present the main ideas of the non-Hermitian-impurity induced waveguide. In Sec. III, we provide a concrete example to illustrate our theory. Section IV demonstrates the dynamics of waveguide in the concrete system. Finally, our conclusion is given in Sec. V.

II. FORMALISM

Consider a bilayer system [Fig. 1(a)], composed of two identical lattices but with opposite on-site energies. The interlayer tunneling is non-Hermitian and sparse, which is referred to as non-Hermitian impurity. The Hamiltonian is given by

$$\begin{aligned} H &= H_0 + H_T, \\ H_0 &= \sum_{\langle i,j\rangle}\sum_{\sigma=\pm}(\kappa_{ij}a^\dagger_{i,\sigma}a_{j,\sigma} + \text{H.c.}) + \sum_j\sum_{\sigma=\pm}\sigma\,\Delta a^\dagger_{j,\sigma}a_{j,\sigma}, \\ H_T &= i\sum_j T_j(a^\dagger_{j,+}a_{j,-} + \text{H.c.}), \end{aligned} \tag{1}$$

where σ corresponds to the $+$ and $-$ layers and $\{iT_j\}$ is a set of imaginary intralayer hopping parameters. Figure 1(a)

*songtc@nankai.edu.cn

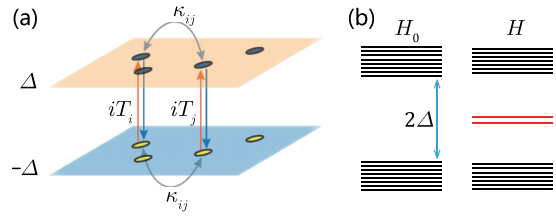

FIG. 1. (a) Schematic illustration of a two-layer tight-binding lattice with non-Hermitian imaginary tunneling. (b) Band structures for H_0 and H. In the absence of the interlayer tunneling, a gap in order of 2Δ opens. When a single tunneling iT_j switches on, two isolated energy levels can be achieved around the midgap.

is the schematic illustration of the model. We consider the region with $\Delta \gg |\kappa_{ij}|$, which ensures the energy gap of order Δ between two $(+/-)$ energy bands for the system H_0. In the following, we show that H_T may induce local states within the energy gap.

In the absence of H_T, the states of H_0 are extended states spreading the probability over the two layers. In the limit case with $|T_j| \sim \Delta \gg |\kappa_{ij}|$, each non-Hermitian tunneling iT_j may induce two isolated energy levels around the midgap, which have the form $\pm\sqrt{\Delta^2 - (T_j)^2}$. It is responsible for the non-Hermiticity of the impurity, since a real tunneling cannot form the isolated levels within the energy gap, but beyond the two bands. Figure 1(b) is the band structure for H_0 and H. We note that the eigenvalues of H are real or imaginary, i.e., the EPs only appear at zero energy. Considering the case with a single nonzero T_j, there are two isolated levels within the gap and such two bound states coalesce to a single state $(1/\sqrt{2})(a^\dagger_{j,-} + ia^\dagger_{j,+})|\text{vac}\rangle$ at the EP when $\Delta = |T_j|$. If there are many such nonzero tunneling T_j within the unbroken region and the corresponding bound states overlap with each other, sub-bands within the gap will form and a non-Hermitian-impurity induced waveguide is achieved for a array of impurity.

To demonstrate the main idea, we consider an example model, which consists of two infinite chains with a single non-Hermitian tunneling. The corresponding Hamiltonian has the form

$$H_{\text{chain}} = \sum_{j=-\infty}^{\infty}\sum_{\sigma=\pm}[(\kappa a^\dagger_{j,\sigma}a_{j+1,\sigma} + \text{H.c.}) + \sigma\Delta a^\dagger_{j,\sigma}a_{j,\sigma}] + iT(a^\dagger_{0,+}a_{0,-} + a^\dagger_{0,-}a_{0,+}), \quad (2)$$

where $\sigma = +$ or $-$ is the index that respectively labels the position in the top or bottom chains and j is the in-chain site index. Parameters κ and T of this model are intra- and interchain hopping strengths. The schematic illustration is shown in Fig. 2(a). Bethe ansatz method shows that there are two bound states around the center with the eigenvector (see Appendix 1)

$$|\psi_{\text{B}}\rangle = C\sum_{j=-\infty}^{\infty}(e^{i\pi j}e^{-\beta^+|j|}a^\dagger_{j,+})|\text{vac}\rangle - C\frac{2\kappa}{iT}\sinh\beta^+\sum_{j=-\infty}^{\infty}(e^{-\beta^-|j|}a^\dagger_{j,-})|\text{vac}\rangle. \quad (3)$$

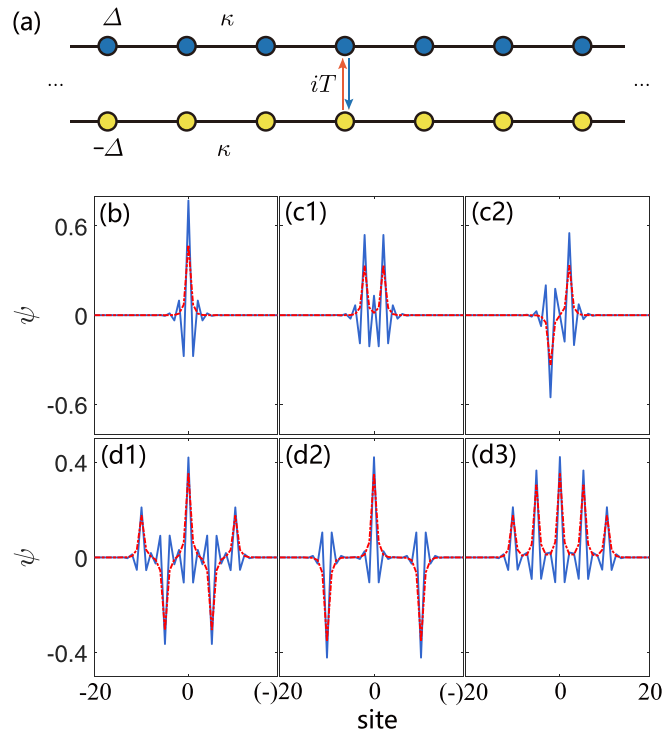

FIG. 2. (a) Schematic illustration of a bichain lattice with opposite chemical potentials $\pm\Delta$ and a single non-Hermitian tunneling iT. The intra- and interlayer hopping strengths are κ and iT, respectively. (b) Profile of one of the two bound states for single imaginary tunneling iT. The ordinates of blue (solid) and red (dash) lines are real and imaginary numbers, which represent the wave function of the top and bottom chains, respectively. The parameters are $\Delta = 5$, $\kappa = 1$, and $T = 4$. Panels (c1) and (c2) are profiles of two of the four bound states for double imaginary tunneling iT. The parameters are $\Delta = 5$, $\kappa = 1$, and $T = 4$. Panels (d1)–(d3) are profiles of three of the ten bound states induced by multi(five) impurities with parameters $\Delta = 5$, $\kappa = 1$, and $T = 4$. The results are obtained by numerical diagonalization and the wave functions are Dirac normalized.

Here C is the normalization coefficient, which is determined in the context of Dirac or biorthogonal inner products. Profile of the bound state is shown in Fig. 2(b). The corresponding eigenenergy is

$$E_{\text{B}} = -2\kappa\cosh\beta^+ + \Delta = 2\kappa\cosh\beta^- - \Delta, \quad (4)$$

where $\beta^\pm$ are positive real numbers and fulfill the equations

$$\cosh\beta^- + \cosh\beta^+ = \Delta/\kappa,$$
$$\sinh\beta^+\sinh\beta^- = T^2/(2\kappa)^2. \quad (5)$$

We note that two bound states coalesce to a single one

$$|\psi^{\text{EP}}_{\text{B}}\rangle = C\sum_{j=-\infty}^{\infty}(e^{i\pi j}e^{-\beta|j|}a^\dagger_{j,+} + ie^{-\beta|j|}a^\dagger_{j,-})|\text{vac}\rangle \quad (6)$$

at EP with $\beta = \ln[\Delta/(2\kappa) + \sqrt{\Delta^2/(4\kappa^2) - 1}]$ and $T = T_{\text{c}} = \sqrt{\Delta^2 - (2\kappa)^2}$. When $T > T_{\text{c}}$, the bound-state energy becomes an imaginary number. This exact solution indicates that stable bound states can be formed by the non-Hermitian impurity. In the case of multi-impurities, the above exact solution is

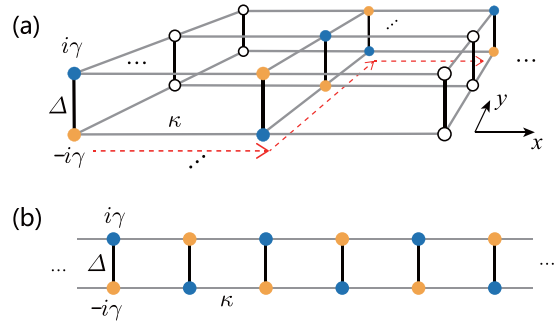

FIG. 3. (a) Schematic illustration of a bilayer square lattice model with κ (gray line) and Δ (black line) are intra- and interlayer hopping strengths; the non-Hermitian imaginary potentials $\pm i\gamma$ are indicated by the blue ($i\gamma$) and yellow ($-i\gamma$) dots, and the white dots indicate zero on-site potentials. (b) The waveguide path [red dash lines in (a)] forms a non-Hermitian ladder model.

still applicable when the distance between two neighboring impurities is sufficiently large. Nevertheless, the overlap of the wave functions occur and extended states form within the region of the impurity array. Figures 2(c) and 2(d) are plots of several typical bound states for two and five imaginary impurities. For n impurities, the system supports $2n$ bound states confined to the region of the array. Consequently, the midgap sub-bands may form for large n.

This result has many implications. (i) Similar to the Hermitian regime, imaginary impurities can induce local bound states with real energies. (ii) In contrast to a Hermitian impurity, energy levels of imaginary impurity can be protected by band gap and coalesce at EP. (iii) Deliberately designed impurity array can take the role of waveguide. It allows a variety of non-Hermitian models with various geometries and a wide range of parameters to be candidates of waveguides. In the next section, we will show its application in an example.

III. BILAYER SQUARE LATTICE

The bound states induced by non-Hermitian impurities can be employed to construct sub-bands in the energy gap, which constitute the channel for specific transport of particle, as a waveguide in a Hermitian system. In the Hermitian realm, the waveguides of most kinds of discrete systems have been well studied. It is usually done by destroying the translational symmetry. In the present work, our strategy is doing the same thing but by adding non-Hermitian terms. In the following, we will present an example that implements a 1D waveguide over a square lattice along any desired path.

We consider a bilayer square lattice model which is shown in Fig. 3(a). The Hamiltonian can be written as the Hermitian part H_0 and non-Hermitian part H_T,

$$H = H_0 + H_T. \tag{7}$$

The corresponding Hermitian Hamiltonian has the form

$$\begin{aligned} H_0 &= H_1 + H_2 + H_{12}, \\ H_\lambda &= \kappa \sum_{j,l} \alpha^\dagger_{j,l,\lambda}(\alpha_{j+1,l,\lambda} + \alpha_{j,l+1,\lambda}) + \text{H.c.}, \\ H_{12} &= \Delta \sum_{j,l} \alpha^\dagger_{j,l,1}\alpha_{j,l,2} + \text{H.c.}, \end{aligned} \tag{8}$$

where $\lambda = 1$ or 2 is the index that respectively labels the position in the top or bottom layers and (j, l) is the in-plane site index. Parameters κ and Δ of this model are intra- and interlayer hopping strengths. And the distribution of imaginary potentials is given as the form

$$H_T = i \sum_{\lambda=1}^{2} \sum_{j,l} (-1)^{\lambda+j+l} \gamma_{jl} \alpha^\dagger_{j,l,\lambda}\alpha_{j,l,\lambda}. \tag{9}$$

By taking the linear transformations

$$a^\dagger_{j,l,\pm} = \frac{1}{\sqrt{2}}(\alpha^\dagger_{j,l,1} \pm \alpha^\dagger_{j,l,2}), \tag{10}$$

the Hamiltonian Eq. (8) can be written as

$$\begin{aligned} H_0 = \kappa \sum_{j,l} \sum_{\sigma=\pm} a^\dagger_{j,l,\sigma}(a_{j+1,l,\sigma} + a_{j,l+1,\sigma}) + \text{H.c.} \\ + \Delta \sum_{j,l} \sum_{\sigma=\pm} \sigma a^\dagger_{j,l,\sigma} a_{j,l,\sigma}. \end{aligned} \tag{11}$$

We note that the bond (antibond) state of a rung can only be transited to the bond (antibond) state next to it with hopping strength κ. Therefore, it can be decomposed into two independent single layer square lattices with on-site potentials Δ and $-\Delta$, respectively.

Accordingly, the non-Hermitian term reads

$$H_T = i \sum_{j,l} (-1)^{j+l+1} \gamma_{j,l} (a^\dagger_{j,l,+} a_{j,l,-} + \text{H.c.}), \tag{12}$$

which takes the role of interlayer imaginary tunneling. Obviously, the present model is a concrete example of the system depicted in Eq. (1). The obtained result is applicable to a wide kind of systems.

IV. DYNAMICS IN WAVEGUIDE

Before proceeding, we present a general non-Hermitian model which exhibits Dirac-probability preserving dynamics. Considering a chiral symmetric system, the Hamiltonian can be written in the block off-diagonal form [41]

$$H = \begin{pmatrix} 0 & D \\ D^\dagger & 0 \end{pmatrix}, \tag{13}$$

where D as an arbitrary $N \times N$ matrix. The basis in H can be a complete set of site states for a bipartite lattice. Based on H as the original Hermitian Hamiltonian, a non-Hermitian Hamiltonian $\mathcal{H}$ is generated as the form

$$\mathcal{H} = H + i\gamma\sigma_z \otimes I_N, \tag{14}$$

where σ_z is the Pauli matrix and I_N denotes the $N \times N$ identity matrix. The chiral symmetry of H ensures its eigenvalues and eigenvectors have the following properties. (i) The eigenvalues are always in pairs, i.e., the spectrum has the form $\{\varepsilon_n, \varepsilon_{-n}\}$ with $\varepsilon_{-n} = -\varepsilon_n$. (ii) The corresponding eigenvector $\{|\phi_n\rangle, |\phi_{-n}\rangle\}$ obeys

$$|\phi_n\rangle = (\sigma_z \otimes I_N)|\phi_{-n}\rangle. \tag{15}$$

It turns out that (see Appendix 2) the spectrum of $\mathcal{H}$ has the form $\{\epsilon_n, \epsilon_{-n}\}$ with

$$\epsilon_{\pm n} = \pm\left(\varepsilon_n^2 - \gamma^2\right)^{1/2} \tag{16}$$

and the eigenvector of $|\varphi_{\pm n}\rangle$ can be mapped directly from $|\phi_{\pm n}\rangle$

$$|\varphi_{\pm n}\rangle = M_{\pm n}|\phi_{\pm n}\rangle \tag{17}$$

with the mapping matrix

$$M_{\pm n} = \begin{pmatrix} a_{\pm n} I_N & 0 \\ 0 & I_N \end{pmatrix}, \tag{18}$$

where $a_{\pm n} = [\epsilon_{\pm n} + i\gamma]/\varepsilon_{\pm n}$ is a complex number with unit modulus, $|a_{\pm n}| = 1$, for real $\epsilon_{\pm n}$.

Obviously, $M_{\pm n}$ is a unitary matrix when the spectrum is fully real. Remarkably, it can be proved that eigenvector set $\{|\varphi_{\pm n}\rangle\}$ obeys a quasiorthonormal relation under the Dirac inner product, i.e.,

$$\langle\varphi_m|\varphi_n\rangle = \delta_{mn}, \tag{19}$$

for $mn > 0$ and $\epsilon_m\epsilon_n \neq 0$. It indicates that the non-Hermitian system acts as a Hermitian one when only one of the subspaces with positive or negative spectrum is concerned. A direct conclusion is that the evolved state in one of the subspace of $\mathcal{H}$ maintains the preservation of Dirac probability, exhibiting the Hermitian dynamic behavior.

Based on the above analysis, the bilayer system is a candidate for waveguide allowing quantum transport with probability preserving. We take the waveguide array by a collection of sites $\{(j, l)\}$ and setting $\gamma_{j,l} = \gamma$, but zero for the rest of sites. In this paper, the set of sites $\{(j, l)\}$ is selected under the rule: it forms a non-Hermitian ladder system, described by the Hamiltonian

$$H_{\text{ladd}} = \kappa \sum_{\lambda=1,2}\sum_{n=1}^{N} \alpha^{\dagger}_{n,\lambda}\alpha_{n+1,\lambda} + \Delta \sum_{n=1}^{N} \alpha^{\dagger}_{n,1}\alpha_{n,2} + \text{H.c.} + \sum_{n=1}^{N} (-1)^n i\gamma(\alpha^{\dagger}_{n,1}\alpha_{n,1} - \alpha^{\dagger}_{n,2}\alpha_{n,2}). \tag{20}$$

The scheme is schematically illustrated in Fig. 3(b). There are numerous configurations for the path to connect any two distant locations. When the parameters are in the range $\gamma \sim \Delta \gg |\kappa|$, the subsystem H_{ladd} decouples from the bilayer system. The dynamics in the waveguide array is governed by the Hamiltonian H_{ladd}. In certain parameter regions, H_{ladd} possesses a fully real spectrum and obeys the Hermitian dynamics since it has the form of Eq. (14).

The system H_{ladd} can be regarded as an extended non-Hermitian SSH chain with long-range hopping term (see Appendix 3). It turns out that such a model shares the same dynamic behaviors with the simplest non-Hermitian SSH chain within a certain parameter region (strong dimerization limit), which has been studied in the previous works [42–44]. It is expected that the dynamics of a non-Hermtian SSH chain emerges in the bilayer squrare lattice with preengineered imaginary impurities.

To see waveguide dynamics in the bilayer square lattice system, we perform the numerical simulations. The initial state is taken as the bilayer Gaussian wave packet, which has the form

$$|\psi(0)\rangle = \Omega^{-1/2} \sum_{\lambda=1,2}\sum_{n=1}^{N} e^{-\alpha^2(n-N_c)^2/2} e^{ik_c n} \alpha^{\dagger}_{n,\lambda}|\text{vac}\rangle, \tag{21}$$

where n is the site index along the waveguide array, N_c is the center of the Gaussian wave packet, k_c is the central momentum, and $\Omega = 2\sqrt{\pi}/\alpha$ is the Dirac normalization factor. According to previous work [42–44], the wave packet should propagate along the array without spreading approximately, if the sub-bands are sufficiently separated from the bilayer bands. The evolved state has the form

$$|\psi(t)\rangle = e^{-iHt}|\psi(0)\rangle, \tag{22}$$

which can be computed by exact diagonalization.

The probability distribution at position (i, j) at time t is defined by the sum of the Dirac probabilities of the top and bottom layers

$$p(i, j, t) = \sum_{\lambda=1,2} |\langle i, j, \lambda|\psi(t)\rangle|^2, \tag{23}$$

where $|i, j, \lambda\rangle$ denotes the position state. To demonstrate the efficiency of the waveguide, we define the function

$$P(i, j) = \frac{p(i, j, t)_{\max}}{\left[\sum_t p(i, j, t)\right]_{\max}} \sum_t p(i, j, t) \tag{24}$$

to record the trace of the wave packet. The simulation is performed for the systems far from EP, i.e., the positive and negative waveguide bands are well separated, and two kinds of waveguide configurations: (i) a single path waveguide with two right-angle bends and (ii) a beam splitter with two right-angle bends. Their schematics are shown in Fig. 4(a) and Fig. 5(a). The initial state is a Gaussian wave packet with central momentum $k_c = -\pi/2$. Since it only relates to a single sub-band in the large gap limit, it is expected that the time evolution exhibits a probability preserving behavior approximately. For case (i), the numerical simulation results indicate that the wave packet propagates along the designed waveguide array path as expected. For (ii), it shows that the wave packet splits into two parts after passing through the joint. In both cases, the wave packet is confined within the defects well and transmitted efficiently around the corners. These numerical results demonstrate and verify our theory for quantum transport in a non-Hermitian impurity array.

V. CONCLUSION AND DISCUSSION

In summary, we have studied the formation of band gap bound states induced by a non-Hermitian impurity embedded in a Hermitian system. We have shown that a pair of bound states emerges inside the band gap when a $\mathcal{PT}$ imaginary potential is added in a strongly coupled bilayer and the bound states become strongly localized when the system approaches the exceptional point. Inspired by this, we construct an impurity array which can be described by a non-Hermitian SSH type effective Hamiltonian which possesses $\mathcal{CT}$ symmetry. We establish a theory for a non-Hermitian impurity-induced waveguide, which paves the way for the non-Hermitian device design. As a supplementary material (Appendix 2) for our theory, we first provide a rigorous proof for the features of a $\mathcal{CT}$-symmetric system, including the reality spectrum and quasiorthogonality of the Dirac inner product. We would like to point out that such two conclusions are independent of other requirements for the original Hermitian system, such

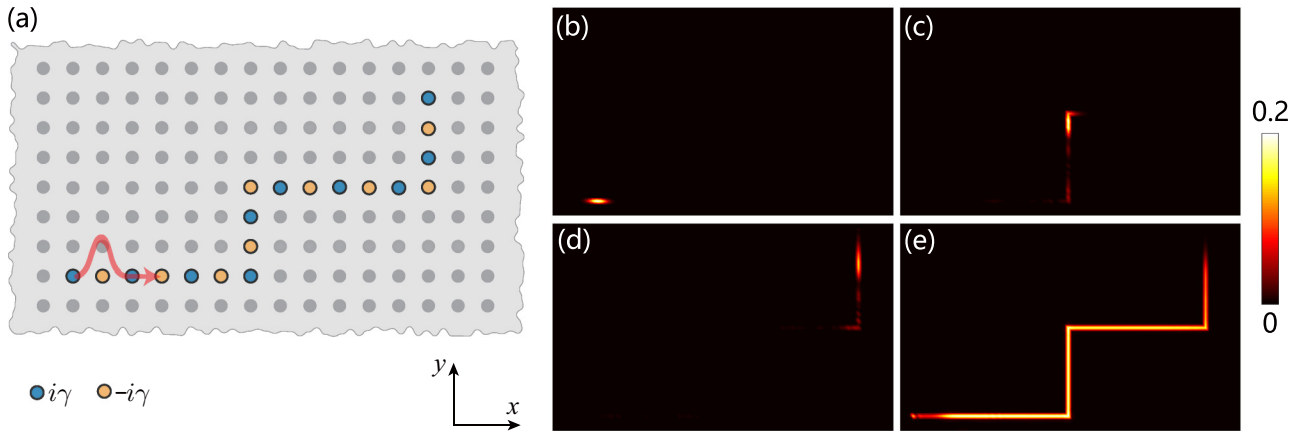

FIG. 4. (a) Schematic illustration of the waveguide path, which is obtained by taking the nonzero non-Hermitian imaginary potentials $\pm i\gamma$ along the path. (b)–(e) Numerical simulations of the dynamics in waveguide. The initial state is a bilayer Gaussian wave packet. Probability distribution at $t = 0$, $t = T_t/2$, and $t = T_t$ are shown in (b), (c), and (d), respectively. (e) The trace of the wave packet. Parameters for the system are $t = 1$, $\Delta = 15$, and $\gamma = 11$; the size of the system is $100 \times 60 \times 2$. Parameters for the initial state Eq. (21) are $\alpha = 0.4$, $N_c = 10$, and $k_c = -\pi/2$. The total duration of the simulation is $T_t = 42J^{-1}$, where J is the scale of the Hamiltonian and we take $J = 1$.

as translational symmetry. Thus a variety of non-Hermitian models with various geometries is allowed. The numerical simulations for the quantum transport of the wave packet in right-angle bends waveguide and Y-beam splitter have demonstrated this point.

ACKNOWLEDGMENTS

This work was supported by National Natural Science Foundation of China (under Grant No. 11874225).

APPENDIX

In this Appendix we present the Bethe ansatz solution for the Hamiltonian from Eq. (2) and properties of the non-Hermitian ladder system.

1. Bound states induced by non-Hermitian impurity

For a single-tunneling non-Hermitian Hamiltonian (2), the bound-state Bethe ansatz wave function has the form

$$|\psi_B\rangle = \sum_{\sigma=\pm}\sum_{j=-\infty}^{\infty} C^{\sigma}(-\sigma)^{|j|}e^{-\beta^{\sigma}|j|}a^{\dagger}_{j,\sigma}|\text{vac}\rangle, \tag{A1}$$

where β^{σ} is a positive real number, indicating the strength of localization around the non-Hermitian tunneling iT. The Schrödinger equation $H_{\text{chain}}|\psi_B\rangle = E_B|\psi_B\rangle$ with bound-state energy E_B gives

$$\begin{aligned} E_B &= -2\kappa\,\cosh\beta^{+} + \Delta \\ &= 2\kappa\,\cosh\beta^{-} - \Delta, \end{aligned} \tag{A2}$$

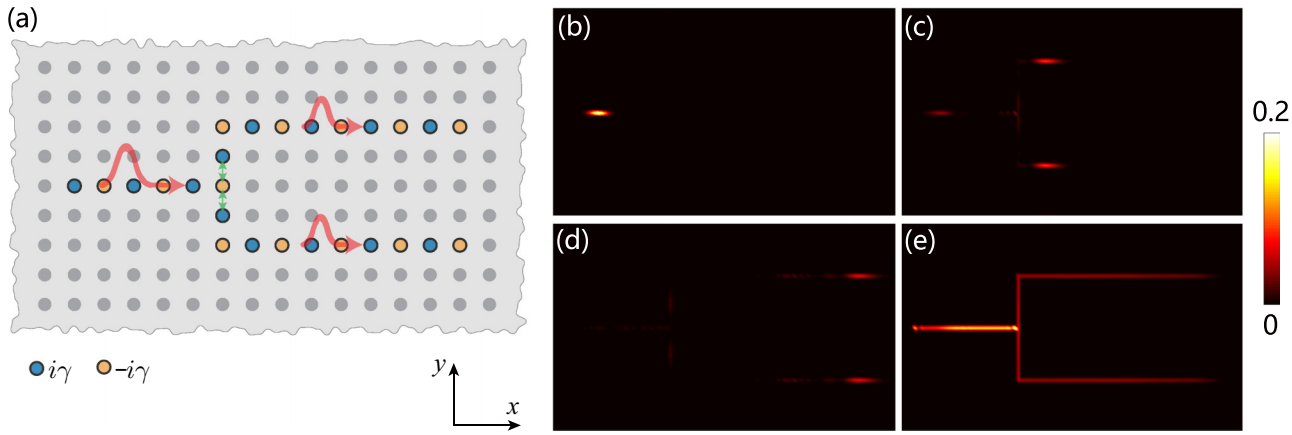

FIG. 5. (a) Schematic illustration of the beam splitter waveguide. In order to get high transmission rate, we take $\kappa \to \kappa/\sqrt{2}$ for the hopping (labeled by green arrows) connecting the joint. (b)–(e) Numerical simulations of the dynamics in waveguide. The initial state is a bilayer Gaussian wave packet. Probability distribution at $t = 0$, $t = T_t/2$, and $t = T_t$ are shown in (b), (c), and (d), respectively. (e) The trace of the wave packet. Parameters for the system are $t = 1$, $\Delta = 15$, and $\gamma = 11$; the size of the system is $100 \times 60 \times 2$. Parameters for the initial state Eq. (21) are $\alpha = 0.4$, $N_c = 10$, and $k_c = -\pi/2$. The total duration of the simulation is $T_t = 32J^{-1}$, where J is the scale of the Hamiltonian and we take $J = 1$.

at $|j| \geqslant 1$, and

$$(\Delta - 2\,e^{-\beta^+}\kappa - E_{\rm B})C^+ + iTC^- = 0,$$
$$iTC^+ + (-\Delta + 2\,e^{-\beta^-}\kappa - E_{\rm B})C^- = 0, \tag{A3}$$

at $j = 0$. The existence of a bound-state solution requires

$$\begin{vmatrix} (\Delta - 2\,e^{-\beta^+}\kappa - E_{\rm B}) & iT \\ iT & (-\Delta + 2\,e^{-\beta^-}\kappa - E_{\rm B}) \end{vmatrix} = 0. \tag{A4}$$

Then evanescent coefficient β^σ can be determined by

$$\cosh\beta^- + \cosh\beta^+ = \Delta/\kappa,$$
$$\sinh\beta^+ \sinh\beta^- = T^2/(2\kappa)^2, \tag{A5}$$

and Eq. (A3) leads to

$$C^\sigma = \frac{2\sigma\kappa}{iT}\sinh\beta^{-\sigma}C^{-\sigma}. \tag{A6}$$

Then the wave function can be written as

$$|\psi_{\rm B}\rangle = \sum_{j=-\infty}^{\infty}(e^{i\pi j}e^{-\beta^+|j|}a^\dagger_{j,+})|{\rm vac}\rangle$$
$$-\frac{2\kappa}{iT}\sinh\beta^+\sum_{j=-\infty}^{\infty}(e^{-\beta^-|j|}a^\dagger_{j,-})|{\rm vac}\rangle, \tag{A7}$$

where the normalization coefficient is neglected since it should be valued in the frameworks of Dirac or biorthonormal inner product in practice. We note that Eq. (A5) is symmetric under the operation $\beta^+ \leftrightarrows \beta^-$. Thus, if $(\beta^+, \beta^-) = (x, y)$ is a solution with the eigenvalue $E_{\rm B}$, then $(\beta^+, \beta^-) = (y, x)$ corresponds to another solution with eigenvalue $-E_{\rm B}$. Accordingly, when we take $T = T_{\rm c} = \sqrt{\Delta^2 - (2\kappa)^2}$, we have $\beta_c = \beta^+ = \beta^-$ with

$$\beta_c = \ln[\Delta/(2\kappa) + \sqrt{\Delta^2/(4\kappa^2) - 1}] \tag{A8}$$

and two bound states coalesce to a single state

$$|\psi_{\rm B}^{\rm EP}\rangle = \sum_{j=-\infty}^{\infty}(e^{i\pi j}e^{-\beta_c|j|}a^\dagger_{j,+} + i\,e^{-\beta_c|j|}a^\dagger_{j,-})|{\rm vac}\rangle, \tag{A9}$$

with the eigenenergy $E_{\rm B}^{\rm EP} = 0$, indicating the occurrence of EP. We note that $|\psi_{\rm B}^{\rm EP}\rangle$ has the identical Dirac probability distributions on the two chains.

In strong localization limit with $e^{2\beta^\sigma} \gg 1$, we have the approximate solutions

$$\begin{pmatrix}\beta^- \\ \beta^+\end{pmatrix} = \begin{pmatrix}\ln(\Delta/\kappa + \sqrt{\Delta^2 - T^2}/\kappa) \\ \ln(\Delta/\kappa - \sqrt{\Delta^2 - T^2}/\kappa)\end{pmatrix}$$
$$\text{or}\begin{pmatrix}\ln(\Delta/\kappa - \sqrt{\Delta^2 - T^2}/\kappa) \\ \ln(\Delta/\kappa + \sqrt{\Delta^2 - T^2}/\kappa)\end{pmatrix}, \tag{A10}$$

which are still in agreement with the symmetry of Eq. (A5).

2. Dirac probability preservation

Consider a Hermitian Hamiltonian with chiral symmetry,

$$H = \begin{pmatrix}0 & D \\ D^\dagger & 0\end{pmatrix}, \tag{A11}$$

where D is an arbitrary $N \times N$ matrix. The Schrödinger equation is

$$H|\phi_{\pm n}\rangle = \varepsilon_{\pm n}|\phi_{\pm n}\rangle \tag{A12}$$

and obeys

$$\varepsilon_{-n} = -\varepsilon_n, \quad |\phi_n\rangle = (\sigma_z \otimes I_N)|\phi_{-n}\rangle, \tag{A13}$$

due to the chiral symmetry

$$\{\sigma_z \otimes I_N, H\} = 0. \tag{A14}$$

A non-Hermitian Hamiltonian $\mathcal{H}$ can be generated as the form

$$\mathcal{H} = H + i\gamma\sigma_z \otimes I_N, \tag{A15}$$

where σ_z is the Pauli matrix and I_N denotes the $N \times N$ identity matrix. We note that a non-Hermitian term breaks the chiral symmetry, but $\mathcal{H}$ has $\mathcal{CT}$ symmetry. The corresponding Schrödinger equation is

$$\mathcal{H}|\varphi_{\pm n}\rangle = \epsilon_{\pm n}|\varphi_{\pm n}\rangle \tag{A16}$$

and obeys

$$\epsilon_{\pm n} = \pm\left(\varepsilon_n^2 - \gamma^2\right)^{1/2}, \quad |\varphi_{\pm n}\rangle = M_{\pm n}|\phi_{\pm n}\rangle, \tag{A17}$$

with the mapping matrix

$$M_{\pm n} = \begin{pmatrix}a_{\pm n}I_N & 0 \\ 0 & I_N\end{pmatrix}, \tag{A18}$$

where $a_{\pm n} = [\epsilon_{\pm n} + i\gamma]/\varepsilon_{\pm n}$ fulfills $|a_{\pm n}| = 1$ for real $\epsilon_{\pm n}$ and is purel imaginary for imaginary $\epsilon_{\pm n}$. For real $\epsilon_{\pm n}$, the factor $a_{\pm n}$ can be written in the form of $a_{\pm n} = e^{i\theta_n}$, with $\theta_n = \arctan(\gamma/\epsilon_{\pm n})$. This can be shown as the following.

Actually, from

$$HM_{\pm n} = \begin{pmatrix}I_N & 0 \\ 0 & a_{\pm n}I_N\end{pmatrix}H, \tag{A19}$$

we have $H|\varphi_{\pm n}\rangle = (HM_{\pm n})|\phi_{\pm n}\rangle$, and

$$H|\varphi_{\pm n}\rangle = \varepsilon_{\pm n}\begin{pmatrix}I_N & 0 \\ 0 & a_{\pm n}I_N\end{pmatrix}|\phi_{\pm n}\rangle$$
$$= \varepsilon_{\pm n}\begin{pmatrix}(a_{\pm n})^{-1}I_N & 0 \\ 0 & a_{\pm n}I_N\end{pmatrix}|\varphi_{\pm n}\rangle. \tag{A20}$$

Therefore, from

$$\mathcal{H}|\varphi_{\pm n}\rangle = (H + i\gamma\sigma_z \otimes I_N)|\varphi_{\pm n}\rangle \tag{A21}$$

and $a_{\pm n} = (\epsilon_{\pm n} + i\gamma)/\varepsilon_{\pm n}$, $\epsilon_{\pm n} = \pm(\varepsilon_n^2 - \gamma^2)^{1/2}$, we have $\varepsilon_{\pm n}(a_{\pm n})^{-1} + i\gamma = \varepsilon_{\pm n}a_{\pm n} - i\gamma = \epsilon_{\pm n}$, which leads to

$$\mathcal{H}|\varphi_{\pm n}\rangle = \epsilon_{\pm n}|\varphi_{\pm n}\rangle. \tag{A22}$$

The mapping relation between vectors $|\phi_n\rangle$ and $|\varphi_n\rangle$ can result in many interesting and useful applications. In general, set $\{|\phi_n\rangle\}$ obeys an orthogonal relation in the framework of the Dirac inner product, while set $\{|\varphi_n\rangle\}$ does not due to the non-Hermiticity of $\mathcal{H}$. We will show that $\{|\varphi_n\rangle\}$ still obeys a Dirac orthogonal relation within one of the subspace ($n > 0$ or $n < 0$).

We start with the eigenvector of Hermitian Hamiltonian H, which has the form

$$|\phi_n\rangle = \begin{pmatrix}A_n \\ B_n\end{pmatrix}, \tag{A23}$$

where A_n and B_n are two $N \times 1$ vectors, representing the wave function of sublattices A and B. $\{|\phi_n\rangle\}$ fulfills the orthogonal normalization condition

$$\langle\phi_m|\phi_n\rangle = A_m^\dagger A_n + B_m^\dagger B_n = \delta_{mn}. \tag{A24}$$

The Schrödinger equation of $|\phi_n\rangle$ has the form

$$\begin{pmatrix} 0 & D \\ D^\dagger & 0 \end{pmatrix}\begin{pmatrix} A_n \\ B_n \end{pmatrix} = \varepsilon_n \begin{pmatrix} A_n \\ B_n \end{pmatrix} \tag{A25}$$

or explicitly

$$\begin{aligned} DB_n &= \varepsilon_n A_n, \\ D^\dagger A_n &= \varepsilon_n B_n. \end{aligned} \tag{A26}$$

Multiplying by $A_m^\dagger$ or $B_m^\dagger$, respectively, we have

$$\begin{aligned} A_m^\dagger D B_n &= \varepsilon_n A_m^\dagger A_n, \\ B_m^\dagger D^\dagger A_n &= \varepsilon_n B_m^\dagger B_n. \end{aligned} \tag{A27}$$

Considering the conjugation of the above Schrödinger equation (A26)

$$\begin{aligned} B_m^\dagger D^\dagger &= \varepsilon_m A_m^\dagger, \\ A_m^\dagger D &= \varepsilon_m B_m^\dagger, \end{aligned} \tag{A28}$$

Eq. (A27) together with Eq. (A28) gives

$$\begin{aligned} \varepsilon_m B_m^\dagger B_n &= \varepsilon_n A_m^\dagger A_n, \\ \varepsilon_m A_m^\dagger A_n &= \varepsilon_n B_m^\dagger B_n, \end{aligned} \tag{A29}$$

and consequently leads to

$$(\varepsilon_n + \varepsilon_m)(A_m^\dagger A_n - B_m^\dagger B_n) = 0. \tag{A30}$$

In the case of $mn > 0$ and $\varepsilon_n \varepsilon_m \neq 0$, we have

$$A_m^\dagger A_n - B_m^\dagger B_n = 0. \tag{A31}$$

Together with the orthogonal normalization condition Eq. (A24), we obtain

$$A_m^\dagger A_n = B_m^\dagger B_n = \tfrac{1}{2}\delta_{mn}, \tag{A32}$$

which means that eigenvector $|\phi_n\rangle$ has the same Dirac probability in sublattices A and B.

This factor leads to an important conclusion for vector $\{|\varphi_n\rangle\}$: different eigenstates in one of the subspace ($mn > 0$) of $\mathcal{H}$ are still orthogonal. In fact, the mapping matrix gives

$$\begin{aligned} \langle\varphi_m|\varphi_n\rangle &= \langle\phi_m|M_m^\dagger M_n|\phi_n\rangle \\ &= a_m^* a_n A_m^\dagger A_n + B_m^\dagger B_n \\ &= \tfrac{1}{2}(a_m^* a_n + 1)\delta_{mn}. \end{aligned} \tag{A33}$$

In addition, for full real spectrum we have

$$\langle\varphi_m|\varphi_n\rangle = \delta_{mn}, \tag{A34}$$

since M_n is unitary, i.e., $|a_n| = |e^{i\theta_n}| = 1$.

As an application, we will show that for any initial state in one of the subspaces ($n > 0$ or $n < 0$) of the non-Hermitian system $\mathcal{H}$, the time evolution preserves the Dirac probability. Considering an initial state in one of the subspaces with the form $|\psi(t=0)\rangle = \sum_{n=1}^N C_n|\varphi_n\rangle$ with $\sum_{n=1}^N C_n^* C_n = 1$, the evolved state can be written as

$$|\psi(t)\rangle = \sum_{n=1}^N C_n \exp(-i\epsilon_n t)|\varphi_n\rangle. \tag{A35}$$

In the condition of a full real spectrum, the Dirac probability is

$$\begin{aligned} P(t) &= \langle\psi(t)|\psi(t)\rangle \\ &= \sum_{m,n=1}^N C_m^* C_n \exp[i(\epsilon_m - \epsilon_n)t]\langle\varphi_m|\varphi_n\rangle \\ &= 1, \end{aligned} \tag{A36}$$

which maintains the preservation of the Dirac probability, exhibiting the Hermitian dynamic behavior.

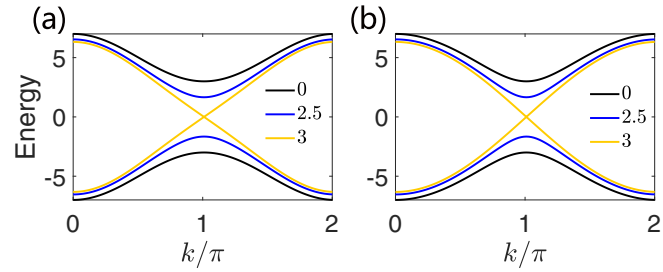

FIG. 6. Spectra of (a) ladder model and (b) SSH model with the core matrix Eq. (A39) and Eq. (A40) for different γ. The Parameters are $\kappa = 1$, $\Delta = 5$, and $\gamma = 0, 2.5, 3$.

3. Non-Hermitian ladder and SSH models

In the condition of $\Delta \gg \kappa$ (strong dimerization limit), the non-Hermitian ladder described by the Hamiltonian in Eq. (20)

$$\begin{aligned} H_{\text{Ladd}} = \kappa \sum_{\lambda=1,2}\sum_{j=1}^N \alpha_{j,\lambda}^\dagger \alpha_{j+1,\lambda} + \Delta \sum_{j=1}^N \alpha_{j,1}^\dagger \alpha_{j,2} + \text{H.c.} \\ + \sum_j (-1)^n i\gamma(\alpha_{j,1}^\dagger \alpha_{j,1} - \alpha_{j,2}^\dagger \alpha_{j,2}) \end{aligned} \tag{A37}$$

is equivalent to a non-Hermitian SSH model

$$\begin{aligned} H_{\text{SSH}} = \sum_{j=1}^N (\Delta a_j^\dagger b_j + 2\kappa a_{j+1}^\dagger b_j) + \text{H.c.} \\ + i\gamma \sum_{j=1}^N (a_l^\dagger a_l - b_l^\dagger b_l). \end{aligned} \tag{A38}$$

Actually, the core matrix of H_{ladd} is

$$h_k^{\text{ladd}} = \begin{pmatrix} i\gamma & \Delta + 2\kappa\cos k \\ \Delta + 2\kappa\cos k & -i\gamma \end{pmatrix}. \tag{A39}$$

For H_{SSH}, we have the core matrix

$$h_k^{\text{SSH}} = \begin{pmatrix} i\gamma & \Delta + 2\kappa e^{-ik} \\ \Delta + 2\kappa e^{ik} & -i\gamma \end{pmatrix}, \tag{A40}$$

which has the same spectrum with

$$h_k = \begin{pmatrix} i\gamma & \sqrt{\Delta^2+4\kappa^2+4\Delta\kappa\ \cos k} \\ \sqrt{\Delta^2+4\kappa^2+4\Delta\kappa\ \cos k} & -i\gamma \end{pmatrix}. \tag{A41}$$

In the case of strong dimerization limit $\Delta^2 \gg \kappa^2$, we have

$$\sqrt{\Delta^2 + 4\kappa^2 + 4\Delta\kappa\ \cos k} \approx \Delta + 2\kappa\ \cos k \tag{A42}$$

or

$$h_k \approx h_k^{\text{ladd}}. \tag{A43}$$

The spectra of ladder model and SSH model with several γ are shown in Figs. 6(a) and 6(b), respectively. It indicates that two spectra are almost identical.

[1] J. D. Joannopoulos, S. G. Johnson, J. N. Winn, and R. D. Meade, *Photonic Crystals: Molding the Flow of Light* (Princeton University Press, Princeton, NJ, 2008).

[2] S. John, Strong Localization of Photons in Certain Disordered Dielectric Superlattices, Phys. Rev. Lett. **58**, 2486 (1987).

[3] E. Yablonovitch, Inhibited Spontaneous Emission in Solid-State Physics and Electronics, Phys. Rev. Lett. **58**, 2059 (1987).

[4] M. Skorobogatiy, G. Bégin, and A. Talneau, Statistical analysis of geometrical imperfections from the images of 2D photonic crystals, Opt. Express **13**, 2487 (2005).

[5] R. J. P. Engelen, D. Mori, T. Baba, and L. Kuipers, Two Regimes of Slow-Light Losses Revealed by Adiabatic Reduction of Group Velocity, Phys. Rev. Lett. **101**, 103901 (2008).

[6] S. Hughes, L. Ramunno, Jeff F. Young, and J. E. Sipe, Extrinsic Optical Scattering Loss in Photonic Crystal Waveguides: Role of Fabrication Disorder and Photon Group Velocity, Phys. Rev. Lett. **94**, 033903 (2005).

[7] E. Kuramochi, M. Notomi, S. Hughes, A. Shinya, T. Watanabe, and L. Ramunno, Disorder-induced scattering loss of line-defect waveguides in photonic crystal slabs, Phys. Rev. B **72**, 161318(R) (2005).

[8] N. Le Thomas, V. Zabelin, R. Houdré, M. V. Kotlyar, and T. F. Krauss, Influence of residual disorder on the anticrossing of Bloch modes probed in k space, Phys. Rev. B **78**, 125301 (2008).

[9] S. Mazoyer, J. P. Hugonin, and P. Lalanne, Disorder-Induced Multiple Scattering in Photonic-Crystal Waveguides, Phys. Rev. Lett. **103**, 063903 (2009).

[10] S. Mazoyer, P. Lalanne, J. C. Rodier *et al.*, Statistical fluctuations of transmission in slow light photonic-crystal waveguides, Opt. Express **18**, 14654 (2010).

[11] L. O'Faolain, T. P. White, D. O'Brien *et al.*, Dependence of extrinsic loss on group velocity in photonic crystal waveguides, Opt. Express **15**, 13129 (2007).

[12] C. M. Bender and S. Boettcher, Real Spectra in Non-Hermitian Hamiltonians having PT Symmetry, Phys. Rev. Lett. **80**, 5243 (1998); C. M. Bender, D. C. Brody, and H. F. Jones, Complex Extension of Quantum Mechanics, *ibid.* **89**, 270401 (2002).

[13] P. Dorey, C. Dunning, and R. Tateo, Spectral equivalences, Bethe ansatz equations, and reality properties in PT-symmetric quantum mechanics, J. Phys. A **34**, 5679 (2001).

[14] A. Mostafazadeh, Pseudo-Hermiticity versus PT symmetry: The necessary condition for the reality of the spectrum of a non-Hermitian Hamiltonian, J. Math. Phys. **43**, 205 (2002); A. Mostafazadeh and A. Batal, Exact PT-symmetry is equivalent to Hermiticity, J. Phys. A **36**, 7081 (2003).

[15] M. Znojil, PT-symmetric harmonic oscillators, Phys. Lett. A **259**, 220 (1999); PT-symmetric square well, **285**, 7 (2001).

[16] H. F. Jones, On pseudo-Hermitian Hamiltonians and their Hermitian counterparts, J. Phys. A **38**, 1741 (2005); Scattering from localized non-Hermitian potentials, Phys. Rev. D **76**, 125003 (2007).

[17] R. El-Ganainy, K. G. Makris, D. N. Christodoulides, and Z. H. Musslimani, Theory of coupled optical PT-symmetric structures, Opt. Lett. **32**, 2632 (2007).

[18] Z. H. Musslimani, K. G. Makris, R. El-Ganainy, and D. N. Christodoulides, Optical Solitons in PT Periodic Potentials, Phys. Rev. Lett. **100**, 030402 (2008).

[19] K. G. Makris, R. El-Ganainy, D. N. Christodoulides, and Z. H. Musslimani, Beam Dynamics in PT Symmetric Optical Lattices, Phys. Rev. Lett. **100**, 103904 (2008).

[20] Y. N. Joglekar, D. Scott, M. Babbey, and A. Saxena, Robust and fragile PT-symmetric phases in a tight-binding chain, Phys. Rev. A **82**, 030103(R) (2010).

[21] D. D. Scott and Y. N. Joglekar, Degrees and signatures of broken PT symmetry in nonuniform lattices, Phys. Rev. A **83**, 050102(R) (2011).

[22] Y. D. Chong, L. Ge, H. Cao, and A. D. Stone, Coherent Perfect Absorbers: Time-Reversed Lasers, Phys. Rev. Lett. **105**, 053901 (2010); Y. D. Chong, L. Ge, and A. D. Stone, PT-Symmetry Breaking and Laser-Absorber Modes in Optical Scattering Systems, *ibid.* **106**, 093902 (2011).

[23] H. Jing, S. K. Özdemir, X.-Y. Lü, J. Zhang, L. Yang, and F. Nori, PT-Symmetric Phonon Laser, Phys. Rev. Lett. **113**, 053604 (2014).

[24] X. Z. Zhang, L. Jin, and Z. Song, Perfect state transfer in PT-symmetric non-Hermitian networks, Phys. Rev. A **85**, 012106 (2012).

[25] X. Z. Zhang, L. Jin, and Z. Song, Self-sustained emission in semi-infinite non-Hermitian systems at the exceptional point, Phys. Rev. A **87**, 042118 (2013).

[26] X. Q. Li, X. Z. Zhang, G. Zhang, and Z. Song, Asymmetric transmission through a flux-controlled non-Hermitian scattering center, Phys. Rev. A **91**, 032101 (2015).

[27] S. Yao and Z. Wang, Edge States and Topological Invariants of Non-Hermitian Systems, Phys. Rev. Lett. **121**, 086803 (2018).

[28] T. Yoshida, R. Peters, and N. Kawakami, Non-Hermitian perspective of the band structure in heavy-fermion systems, Phys. Rev. B **98**, 035141 (2018).

[29] T. Yoshida, R. Peters, N. Kawakami, and Y. Hatsugai, Symmetry-protected exceptional rings in two-dimensional correlated systems with chiral symmetry, Phys. Rev. B **99**, 121101(R) (2019).

[30] T. Yoshida and Y. Hatsugai, Exceptional rings protected by emergent symmetry for mechanical systems, arXiv:1904.10764.

[31] A. Guo, G. J. Salamo, D. Duchesne, R. Morandotti, M. Volatier-Ravat, V. Aimez, G. A. Siviloglou, and D. N. Christodoulides, Observation of PT-Symmetry Breaking in Complex Optical Potentials, Phys. Rev. Lett. **103**, 093902 (2009).

[32] C. E. Rüter *et al.*, Observation of parity–time symmetry in optics, Nat. Phys. **6**, 192 (2010).

[33] W. Wan, Y. Chong, L. Ge, H. Noh, A. D. Stone, and H. Cao, Time-reversed lasing and interferometric control of absorption, Science **331**, 889 (2011).

[34] Y. Sun, W. Tan, H.-Q. Li, J. Li, and H. Chen, Experimental Demonstration of a Coherent Perfect Absorber with PT Phase Transition, Phys. Rev. Lett. **112**, 143903 (2014).

[35] L. Feng *et al.*, Experimental demonstration of a unidirectional reflectionless parity-time metamaterial at optical frequencies, Nat. Mater. **12**, 108 (2013).

[36] B. Peng *et al.*, Parity–time-symmetric whispering-gallery microcavities, Nat. Phys. **10**, 394 (2014).

[37] L. Chang *et al.*, Parity-time symmetry and variable optical isolation in active-passive-coupled microresonators, Nat. Photon. **8**, 524 (2014).

[38] L. Feng, Z. J. Wong, R.-M. Ma, Y. Wang, and X. Zhang, Single-mode laser by parity-time symmetry breaking, Science **346**, 972 (2014).

[39] H. Hodaei *et al.*, Parity-time-symmetric microring lasers, Science **346**, 975 (2014).

[40] M. Wimmer *et al.*, Observation of optical solitons in PT-symmetric lattices, Nat. Commun **6**, 7782 (2015).

[41] C.-K. Chiu, J. C. Y. Teo, A. P. Schnyder, and S. Ryu, Classification of topological quantum matter with symmetries, Rev. Mod. Phys. **88**, 035005 (2016).

[42] W. H. Hu, L. Jin, Y. Li, and Z. Song, Probability-preserving evolution in a non-Hermitian two-band model, Phys. Rev. A **86**, 042110 (2012).

[43] K. L. Zhang, P. Wang, G. Zhang, and Z. Song, Simple harmonic oscillation in a non-Hermitian Su-Schrieffer-Heeger chain at the exceptional point, Phys. Rev. A **98**, 022128 (2018).

[44] K. L. Zhang, P. Wang, and Z. Song, Exceptional-point-induced lasing dynamics in a non-Hermitian Su-Schrieffer-Heeger model, Phys. Rev. A **99**, 042111 (2019).